Detection in Multiple Disparate Systems using Multi-Channel Coherence Analysis

NICK KLAUSNER, Student Member, IEEE
MAHMOOD R. AZIMI-SADJADI, Senior Member, IEEE
Colorado State University

This paper presents a coherence-based detection method for multiple disparate sensing systems using the multi-channel coherence analysis (MCA) framework. MCA provides an optimal coordinate system for multi-channel detection problems as it finds sets of one-dimensional mapping vectors that maximize the sum of the cross-correlations among all pair-wise combinations of channels. The standard detector for Gaussian random vectors is then cast into the MCA framework by developing the log-likelihood ratio and J-divergence measure. The proposed detection method is then tested on a data set consisting of sets of four side-scan sonar images coregistered over the same region on the seafloor and the results are compared with those of a multi-channel generalized likelihood ratio (GLR) detector.

Manuscript received December 22, 2010; revised September 19 and December 12, 2011; released for publication February 15, 2012.

IEEE Log No. T-AES/48/4/944221.

Refereeing of this contribution was handled by W. Blanding.

This work was supported by the Office of Naval Research (ONR) under Contract N00014-09-1-0087.

Authors' address: Department of Electrical and Computer Engineering, Colorado State University, Engineering Room B104, 1373 Campus Delivery, Fort Collins, CO 80523-1373, E-mail: (nklausne@engr.colostate.edu).

I. INTRODUCTION

There are many examples of oceanic applications that rely on the observations from multiple disparate sensing systems to detect various sources of interest. One example is the detection of underwater mine-like objects in multiple side-scan images generated from sonar systems that could be disparate in location, frequency, beamwidth resolution, etc. Typical application of detection systems in such situations often times revolve around a decision fusion technique which combines individual detection decisions into one global decision. However, this detection paradigm can often lead to suboptimal performance as local decisions are made based on the perspective of a single sensory system. To allow collaborative decision-making among multiple sonar platforms, it is essential to detect and further scrutinize the information bearing parts of the data collected by the various sensory systems. This involves detecting, isolating, and representing, in terms of some pertinent attributes, the coherent, or mutual information among one or multiple data sets. Therefore, new methodologies are needed to: 1) collaboratively detect and agree on target activities occurring within the field of view of the sensors, 2) perform feature extraction to capture common target attributes for object classification, and 3) develop a single integrated target assessment picture based upon the detected, localized, and classified targets from multiple disparate sensors.

Multi-channel detection has recently been considered in [1]–[3]. In [1] a nonparametric approach to multi-channel detection is proposed by defining the generalized coherence (GC) measure among N channels using the normalized Grammian matrix of measurements. This measure can then be used to perform binary hypothesis testing for the multi-channel data. Since no a priori assumptions are made about the alternative hypothesis H_1, the estimate applies to a wide range of different signal models. For the null hypothesis H_0, however, it is assumed that the measurements from all N channels are white Gaussian random vectors. Then, the H_0 distribution of the magnitude-squared coherence (MSC) estimate is derived which can effectively be used to find thresholds corresponding to a constant false alarm rate. Under the same assumptions the authors then derived the distribution of the three-channel GC estimate under H_0 leading to a recursive formulation for finding the distribution as one adds an additional channel. The authors note, however, that the GC estimate ignores temporally correlated random processes, and hence, the propagation delays and Doppler shifts must be estimated and accounted for prior to detection. Multi-channel detection for uncalibrated elements in a sensor array is considered in [2] by forming a generalized likelihood ratio test (GLRT) and using the assumption that observations

are zero-mean, complex Gaussian distributed random vectors. The GLRT involves testing whether the sample covariance matrix, computed from a window's worth of data, has diagonal structure (unknown) under H_0 versus any arbitrary, positive-definite (PD) covariance structure under H_1. In this case the GLRT test statistic becomes a Hadamard ratio involving the sample covariance matrix. The authors note that the GLRT presents an advantageous method for performing detection when sensor calibration data is absent. This work is then generalized in [3] by considering a problem where one is given multiple independent copies of a finite-length, vector-valued time series. Vectorizing each copy into a larger dimensional, spatio-temporal random vector and forming a data matrix from all the independent copies of this vector, the sample covariance matrix is estimated. The GLRT then involves testing whether the sample covariance matrix is block-diagonal under H_0 versus any arbitrary PD covariance structure under H_1. With these assumptions, the GLRT test statistic is written in terms of a generalized Hadamard ratio involving the sample covariance matrices or the determinant of the estimated coherence matrix. Making the asymptotic assumption that both the number of temporal measurements and the number of independent copies grow large, the test statistic is then written in terms of the log of the Hadamard ratio involving the estimated power spectral density matrices for each channel, integrated over the Nyquist band. Properties of the proposed detection statistic are given, its relationship to mutual information shown, and a low-correlation regime approximation is then developed.

Recently, canonical correlation analysis (CCA) [4] has been looked at for coherent detection and feature extraction. The canonical coordinate decomposition method not only determines linear dependence [5] or coherence between two data channels but also extracts a subset of the most important coordinates for low-rank detection [6]. The CCA method has shown great promise in underwater target classification problems using sonar backscatter data [7]. In this work the canonical correlations extracted from the time series corresponding to pairs of sonar returns were shown to have high discriminatory power for both detection and classification. These studies were then extended and improved upon in [8] by measuring coherence between the same frequency band in two sonar pings. CCA was utilized in [9] to form a dual channel detector in which detection decisions are based on the amount of coherent information shared among pairs of coregistered regions of interest (ROIs) from two different sonar images. The results of applying the detector to a distributed detection problem in which the decisions from two individual detectors were fused exhibited a much lower false alarm rate and higher probability of detection when compared with the results of each individual detector applied independently to the same data set.

Multi-channel coherence analysis (MCA) [10, 11] can be seen as a natural extension of CCA to more than two channels. MCA-based decomposition similarly looks for sets of one-dimensional mappings that maximize the sum of the cross-correlations among any number of channels. In [12] MCA is applied to Landsat imagery to quantify the amount of coherent information from multiple spectral bands and across different images in time. In [11] an iterative procedure for performing the MCA decomposition and finding the coordinates and correlations is proposed. Similarly, in [13] a generalization of CCA to several data sets is proposed and shown to be equivalent to the classical maximum variance generalization proposed in [10]. Reformulating the problem as a set of coupled least squares regression problems, the proposed generalization is implemented via a two-layer feedforward neural network which is trained using a recursive least squares algorithm. The convergence of the proposed learning rule is proved by means of stochastic approximation techniques and its performance is then analyzed through simulation.

The goal of this paper is to develop an efficient and robust coherence-based detection system for multiple sensor platforms that maintains good performance in varying operating and environmental conditions. The developed system is then applied to underwater target detection from multiple side-scan sonar imagery. For this system, our detection hypothesis is that the presence of a target in coregistered ROIs from multiple sonar images will exhibit different levels of coherence than when ROIs contain only background. Based on this detection hypothesis, we construct a simple multi-channel detection problem which is then solved via MCA and cast into the standard Gauss-Gauss detection framework. The work presented here will develop the log-likelihood ratio and J-divergence for the composite multi-channel hypothesis test in the MCA framework. Test results on a data set containing one high frequency (HF) and three broadband (BB) sonar imagery coregistered over the seafloor are then provided. This data set is used to examine different combinations of these sonar images, construct three different multi-channel detectors with the HF image and one or more BB images, and compare detection performance as a function of the number of sonar images used. The results of the MCA-based detection method are also compared with the GLRT proposed in [3]. As we see later, both methods inherently rely on the same detection hypothesis with the only difference being the test statistics used to form detection decisions.

This paper is organized as follows. Section II reviews the MCA algorithm and discusses some of the properties of the MCA variates. Section III

establishes the hypothesis test for this problem and extends the standard Gauss-Gauss detector into the MCA framework. Section IV provides a description of the multi-sonar data set, describes the preprocessing steps used to prepare the data for the MCA detector, and presents the results. Concluding remarks are then made in Section V.

II. MCA REVIEW

Consider N zero-mean random vectors, $\mathbf{x}_1, \mathbf{x}_2, \ldots$, and $\mathbf{x}_N$, representing multiple data channels comprising the composite data channel $\mathbf{z} = [\mathbf{x}_1^H \mathbf{x}_2^H \cdots \mathbf{x}_N^H]^H \in \mathbb{C}^{d\times 1}$. Let each channel $\mathbf{x}_j \in \mathbb{C}^{d_j \times 1}$ be of dimension d_j with $d = \sum_{j=1}^N d_j$. The $d \times d$ dimensional covariance matrix of the composite data channel $\mathbf{z}$ is given by

$$R_{\mathbf{zz}} = E[\mathbf{z}\mathbf{z}^H] = \begin{bmatrix} R_{11} & R_{12} & \cdots & R_{1N} \\ R_{21} & R_{22} & \cdots & R_{2N} \\ \vdots & \vdots & \ddots & \vdots \\ R_{N1} & R_{N2} & \cdots & R_{NN} \end{bmatrix} \tag{1}$$

where $R_{jk} = E[\mathbf{x}_j \mathbf{x}_k^H]$ is the auto-covariance ($j = k$) or cross-covariance ($j \neq k$) matrices of data channels $\mathbf{x}_j$ and $\mathbf{x}_k$ and we have $R_{jk} = R_{kj}^H$. No specific structure is assumed for $R_{\mathbf{zz}}$ with the only assumption that it is PD.

Similar to two-channel CCA [4] the ith multi-channel coordinate of the jth channel is found by searching for the ith coordinate mapping vector $\boldsymbol{\alpha}_{i,j}$ of data channel $\mathbf{x}_j$. This linear transformation produces the ith multi-channel coordinate for the jth channel,

$$v_{i,j} = \boldsymbol{\alpha}_{i,j}^H \mathbf{x}_j. \tag{2}$$

If the ith coordinate mapping vectors are found for all N channels, we obtain the composite coordinate mapping vector $\mathbf{a}_i = [\boldsymbol{\alpha}_{i,1}^H \ \boldsymbol{\alpha}_{i,2}^H \cdots \boldsymbol{\alpha}_{i,N}^H]^H$. This is then used to find the composite coordinate vector $\mathbf{v}_i = [v_{i,1} \ v_{i,2} \cdots v_{i,N}]^T$ which consists of the ith multi-channel coordinate of every channel. The associated covariance matrix of $\mathbf{v}_i$ is given by

$$R_{\mathbf{v}_i\mathbf{v}_i} = \begin{bmatrix} \boldsymbol{\alpha}_{i,1}^H R_{11} \boldsymbol{\alpha}_{i,1} & \cdots & \boldsymbol{\alpha}_{i,1}^H R_{1N} \boldsymbol{\alpha}_{i,N} \\ \vdots & \ddots & \vdots \\ \boldsymbol{\alpha}_{i,N}^H R_{N1} \boldsymbol{\alpha}_{i,1} & \cdots & \boldsymbol{\alpha}_{i,N}^H R_{NN} \boldsymbol{\alpha}_{i,N} \end{bmatrix}. \tag{3}$$

Recall that in the two-channel CCA [4] the first coordinate is obtained by maximizing the correlation among the two mapped variates while constraining them to have unit variance. Subsequent coordinates are then similarly found with the added constraint that they be uncorrelated with the previous coordinates. In the multi-channel case, however, the analysis is not as well defined as all correlations between all possible pairs of channels must be maximized simultaneously. To accomplish this, one approach [12] is to maximize the sum of all correlations subject to the unit trace constraint of matrix $R_{\mathbf{v}_i\mathbf{v}_i}$. Thus, the optimization problem for finding the 1st composite coordinate mapping vector $\mathbf{a}_1$ becomes

$$\begin{aligned} \mathbf{a}_1 &= \arg\max_{\mathbf{a}_1} \sum_{j=1}^N \sum_{k=1}^N \boldsymbol{\alpha}_{1,j}^H R_{j,k} \boldsymbol{\alpha}_{1,k} \\ &= \arg\max_{\mathbf{a}_1} \sum_{j=1}^N \sum_{k=1}^N [R_{\mathbf{v}_1\mathbf{v}_1}]_{j,k} \end{aligned}$$

subject to the constraint

$$\operatorname{tr}(R_{\mathbf{v}_1\mathbf{v}_1}) = \sum_{j=1}^N \boldsymbol{\alpha}_{1,j}^H R_{jj} \boldsymbol{\alpha}_{1,j} = \sum_{j=1}^N [R_{\mathbf{v}_1\mathbf{v}_1}]_{j,j} = 1.$$

It can easily be shown [12] that the above constrained optimization problem for finding the mapping vectors $\boldsymbol{\alpha}_{1,j}$s using a Lagrange multiplier method leads to

$$\sum_{k=1}^N R_{jk} \boldsymbol{\alpha}_{1,k} = \lambda_1 R_{jj} \boldsymbol{\alpha}_{1,j}$$

or in matrix notation as

$$R_{\mathbf{zz}} \mathbf{a}_1 = \lambda_1 D \mathbf{a}_1 \tag{4}$$

where D is a block diagonal matrix with diagonal blocks R_{jj}, $\forall j \in [1,N]$, i.e., $D = \operatorname{diag}[R_{11}, R_{22}, \ldots, R_{NN}]$. Simply left-multiplying (4) by $\mathbf{a}_1^H$ and recalling that $\mathbf{a}_1^H D \mathbf{a}_1 = \sum_{j=1}^N \boldsymbol{\alpha}_{1,j}^H R_{jj} \boldsymbol{\alpha}_{1,j}^H$ is constrained to equal 1 yields $\lambda_1 = \mathbf{a}_1^H R_{\mathbf{zz}} \mathbf{a}_1 = \sum_{j=1}^N \sum_{k=1}^N E[v_{1,j} v_{1,k}^*]$ which implies that each Lagrange multiplier is the sum of the correlations among all mapped variates.

The result of (4) represents a generalized eigenvalue problem for which standard methods of solution are well known [14]. Subsequent coordinates ($i > 1$) are found by enforcing additional orthogonality constraints, i.e., $\mathbf{a}_i^H R_{\mathbf{zz}} \mathbf{a}_q = \sum_{j=1}^N \sum_{k=1}^N E[v_{i,j} v_{q,k}^*] = 0$ for all $q < i$. Finding the solution for all mapping vectors $\mathbf{a}_i$s, $i \in [1,d]$, we write (4) as $R_{\mathbf{zz}} A = D A \Lambda$ where $A = [\mathbf{a}_1 \ \mathbf{a}_2 \cdots \mathbf{a}_d]$ consists of all d coordinate mapping vectors, and $\Lambda = \operatorname{diag}[\lambda_1, \lambda_2, \ldots, \lambda_d]$ consists of all d eigenvalues. Since both $R_{\mathbf{zz}}$ and D represent symmetric covariance matrices and further D is PD, the solution can then be rewritten in terms of a standard eigenvalue decomposition (EVD)

$$EP = P\Lambda \tag{5}$$

where $E = D^{-1/2} R_{\mathbf{zz}} D^{-H/2}$ and $P = D^{H/2} A$. Since E, which we refer to as the coherence matrix, is also symmetric all eigenvalues are guaranteed [14] to be real-valued and P is a unitary matrix, i.e., $P^H P = P P^H = I$. Clearly, we may then extract the matrix A via $A = D^{-H/2} P$.

Inspection of matrix E shows that it is simply the composite covariance matrix of the whitened

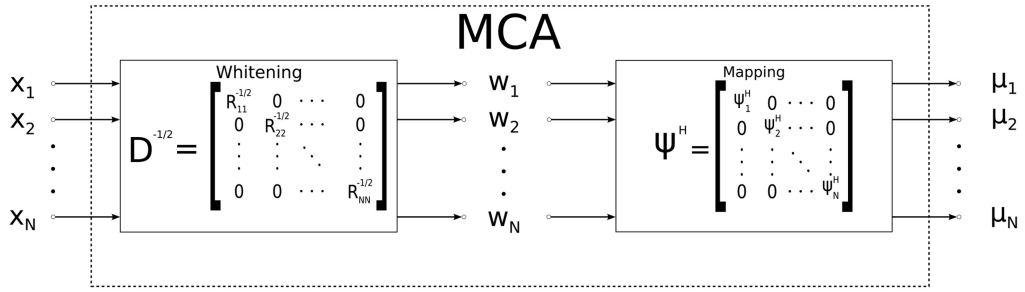

Fig. 1. MCA processing block diagram.

version of $\mathbf{z} = [\mathbf{x}_1^H \cdots \mathbf{x}_N^H]^H$. That is, if we define this whitened version of the composite data channel vector by $\mathbf{w} = [\mathbf{w}_1^H \cdots \mathbf{w}_N^H]^H = D^{-1/2}\mathbf{z}$ where $E[\mathbf{w}_j\mathbf{w}_j^H] = I_{d_j}$ and $E[\mathbf{w}_j\mathbf{w}_k^H] = R_{jj}^{-1/2}R_{jk}R_{kk}^{-H/2}$, then the whitened composite vector $\mathbf{w}$ has correlation matrix $E[\mathbf{w}\mathbf{w}^H] = D^{-1/2}R_{\mathbf{zz}}D^{-H/2} = E$. Matrix P is then used to map the whitened channels to their multi-channel coordinates and is structured in the following fashion

$$P = [\mathbf{p}_1 \quad \mathbf{p}_2 \cdots \mathbf{p}_d] = \begin{bmatrix} \mathbf{p}_{1,1} & \mathbf{p}_{2,1} & \cdots & \mathbf{p}_{d,1} \\ \mathbf{p}_{1,2} & \mathbf{p}_{2,2} & \cdots & \mathbf{p}_{d,2} \\ \vdots & \vdots & \ddots & \vdots \\ \mathbf{p}_{1,N} & \mathbf{p}_{2,N} & \cdots & \mathbf{p}_{d,N} \end{bmatrix}.$$

To find the mapped coordinate vector $\mathbf{v}$ that contains all mapped coordinates for all N channels, we first define matrix Ψ_j (dimension $d_j \times d$) to contain the portion of the mapping matrix P that corresponds to the j^{th} channel, i.e.,

$$\Psi_j = [\mathbf{p}_{1,j} \quad \mathbf{p}_{2,j} \cdots \mathbf{p}_{d,j}], \qquad \forall j \in [1,N]. \tag{6}$$

Clearly, the connection between P and Ψ_j is evident

$$P = \begin{bmatrix} \Psi_1 \\ \Psi_2 \\ \vdots \\ \Psi_N \end{bmatrix}_{d \times d}. \tag{7}$$

All of the mapped coordinates of the jth channel can then be found by

$$\boldsymbol{\mu}_j = \Psi_j^H \mathbf{w}_j = \Psi_j^H R_{jj}^{-1/2}\mathbf{x}_j, \qquad \forall j \in [1,N] \tag{8}$$

where $\boldsymbol{\mu}_j = [v_{1,j} \quad v_{2,j} \cdots v_{d,j}]^T$. These coordinates exhibit the following properties

$$\begin{aligned} \sum_{j=1}^{N} E[\boldsymbol{\mu}_j\boldsymbol{\mu}_j^H] &= \sum_{j=1}^{N} \Psi_j^H\Psi_j \\ &= P^HP = A^HDA = I \\ \sum_{j=1}^{N}\sum_{k=1}^{N} E[\boldsymbol{\mu}_j\boldsymbol{\mu}_k^H] &= \sum_{j=1}^{N}\sum_{k=1}^{N} \Psi_j^H R_{jj}^{-1/2}R_{jk}R_{kk}^{-H/2}\Psi_k \\ &= P^HEP = A^HR_{\mathbf{zz}}A = \Lambda. \end{aligned} \tag{9}$$

The first equation confirms the fact that all d coordinates satisfy the unit trace constraint. Likewise, the second equation restates the fact that the sum of the correlations of the mapped variates is matrix Λ and the coordinates are orthogonal, i.e., $\mathbf{a}_i^HR_{\mathbf{zz}}\mathbf{a}_q = \delta_{i-q}\lambda_i$ for all $i,q \in [1,d]$.

If we define block diagonal matrix $\boldsymbol{\Psi}$ that contains the Ψ_j matrices along its diagonal blocks, i.e., $\boldsymbol{\Psi} = \text{diag}[\Psi_1, \Psi_2, \ldots, \Psi_N]$, then we can resolve all N channels into their multi-channel coordinates using

$$\mathbf{v} = [\boldsymbol{\mu}_1^H \quad \boldsymbol{\mu}_2^H \cdots \boldsymbol{\mu}_N^H]^H = \boldsymbol{\Psi}^H\mathbf{w} = \boldsymbol{\Psi}^HD^{-1/2}\mathbf{z}. \tag{10}$$

Figure 1 displays the process behind the MCA analysis filter. As can be seen, similar to CCA [4], all channels are first whitened in order to remove the auto-correlation contributions from each individual channel. Each whitened channel is then mapped to its MCA coordinate via matrix $\boldsymbol{\Psi}$ thereby allowing one to analyze the linear dependence shared among the channels.

REMARK 1 The sum of all d eigenvalues equals d itself, i.e.,

$$\begin{aligned} \sum_{i=1}^{d}\lambda_i &= \text{tr}(P^HEP) = \text{tr}(E) = \text{tr}(D^{-1}R_{\mathbf{zz}}) \\ &= \sum_{j=1}^{N}\text{tr}(I_{d_j}) = \sum_{j=1}^{N} d_j = d \end{aligned} \tag{11}$$

where I_{d_j} denotes an identity matrix of dimension d_j.

REMARK 2 Each eigenvalue, $\lambda_i \geq 0$, can never grow larger than the number of channels N, i.e., $0 \leq \lambda_i \leq N$. To see this, we use the Cauchy-Schwarz inequality

$$\begin{aligned} \lambda_i &= \left|\sum_{j=1}^{N}\sum_{k=1}^{N} E[v_{i,j}v_{i,k}^*]\right| \\ &\leq \sum_{j=1}^{N}\sum_{k=1}^{N} |E[v_{i,j}v_{i,k}^*]| \\ &\leq \sum_{j=1}^{N}\sum_{k=1}^{N} \sqrt{E[|v_{i,j}|^2]E[|v_{i,k}|^2]} \end{aligned}$$

with the upper bound attained if and only if $v_{i,k} = v_{i,j}$ $\forall j \neq k$ almost surely, in which case we can write

$$\lambda_i \leq \sum_{k=1}^{N}\sum_{j=1}^{N} E[|v_{i,j}|^2].$$

Now, recalling that each coordinate is constrained to satisfy the unit trace constraint, i.e., $\sum_{j=1}^{N} E[|v_{i,j}|^2] = \sum_{j=1}^{N} \boldsymbol{\alpha}_{i,j}^H R_{jj} \boldsymbol{\alpha}_{i,j} = 1$, and the fact that matrix E is PD, it then easily follows that $0 \leq \lambda_i \leq N$.

REMARK 3 In the special case that $N = 2$ and assuming with no loss in generality that $d_1 \leq d_2$, the matrix E can be written as

$$E = \begin{bmatrix} I_{d_1} & C \\ C^H & I_{d_2} \end{bmatrix}$$

where $C = R_{11}^{-1/2} R_{12} R_{22}^{-H/2} \in \mathbb{C}^{d_1 \times d_2}$ is a matrix commonly referred as the coherence matrix [5, 6] in the two-channel CCA which motivates referring to E as the coherence matrix for multi-channel MCA. Each multi-channel correlation λ_i is a root of the characteristic polynomial satisfying $\det(\lambda I_d - E) = 0$ which can be rewritten

$$(\lambda - 1)^{d_2 - d_1} \det[\xi I_{d_1} - CC^H] = 0$$

where $\xi = (\lambda - 1)^2$ is an eigenvalue of the squared coherence matrix CC^H which are known [5, 6] to be squared canonical correlations k^2 in two-channel CCA. Given the canonical correlations $\{k_i\}_{i=1}^{d_1}$, this equation shows us that there are d_1 correlations of the form $\lambda_i = 1 + k_i$, d_1 correlations of the form $\lambda_i = 1 - k_i$, and $d_2 - d_1$ correlations which are deterministically set to unity, i.e., $\lambda_i = 1$. Recalling the results in Remarks 1 and 2, we note that $\sum_{i=1}^{d} \lambda_i = d$ and, using the fact that $0 \leq k_i \leq 1$, we can see that $0 \leq \lambda_i \leq 2$.

III. MCA-BASED DETECTION

We now turn our attention to MCA-based detection. For this multi-sonar problem, we assume that the observations from all N channels consist of uncorrelated realizations of background noise under H_0 versus the hypothesis that our observations contain correlated signal components corrupted by additive noise. More specifically, for the jth platform we consider the signal-plus-noise model

$$H_1: \quad \mathbf{x}_j = \mathbf{s}_j + \mathbf{n}_j$$

$$H_0: \quad \mathbf{x}_j = \mathbf{n}_j$$

where $\mathbf{n}_j \in \mathbb{C}^{d_j}$ and $\mathbf{s}_j \in \mathbb{C}^{d_j}$ are both zero-mean, proper complex Gaussian random vectors with the auto- and cross-covariance matrices $E[\mathbf{n}_j \mathbf{n}_k^H] = \delta_{j-k} R_{\mathbf{n}_j}$, $E[\mathbf{s}_j \mathbf{s}_k^H] = R_{\mathbf{s}_j \mathbf{s}_k}$, and $E[\mathbf{s}_j \mathbf{n}_k^H] = \mathbf{O}$ for all $j,k = 1,\ldots,N$.

Under H_0, since the realizations of noise were assumed to be uncorrelated across different channels, we have

$$R_{\mathbf{zz}_0} = D_0 = \mathrm{diag}[R_{\mathbf{n}_1}, R_{\mathbf{n}_2}, \ldots, R_{\mathbf{n}_N}]$$

where the subscript notation refers to the hypothesis being considered.

Under H_1 the corresponding composite covariance matrix $R_{\mathbf{zz}}$ and block diagonal matrix D become

$$R_{\mathbf{zz}_1} = \begin{bmatrix} R_{\mathbf{s}_{11}} + R_{\mathbf{n}_1} & \cdots & R_{\mathbf{s}_{1N}} \\ R_{\mathbf{s}_{21}} & \cdots & R_{\mathbf{s}_{2N}} \\ \vdots & \ddots & \vdots \\ R_{\mathbf{s}_{N1}} & \cdots & R_{\mathbf{s}_{NN}} + R_{\mathbf{n}_N} \end{bmatrix}$$

and

$$D_1 = \mathrm{diag}[R_{\mathbf{s}_{11}} + R_{\mathbf{n}_1}, \ldots, R_{\mathbf{s}_{NN}} + R_{\mathbf{n}_N}].$$

Recalling (4), this leads to the following eigenvalue decomposition for the H_1 hypothesis

$$R_{\mathbf{zz}_1} A_1 = D_1 A_1 \Lambda_1. \tag{12}$$

Noting that we can alternatively write the inverse of the covariance matrix under hypothesis H_1 as

$$R_{\mathbf{zz}_1}^{-1} = D_1^{-H/2} P_1 \Lambda_1^{-1} P_1^H D_1^{-1/2}$$

where $P_1 = D_1^{H/2} A_1$, the log-likelihood ratio [15] can be written as

$$\begin{aligned} l(\mathbf{z}) &= \mathbf{z}^H (R_{\mathbf{zz}_0}^{-1} - R_{\mathbf{zz}_1}^{-1}) \mathbf{z} \\ &= \mathbf{z}^H (D_0^{-1} - D_1^{-H/2} P_1 \Lambda_1^{-1} P_1^H D_1^{-1/2}) \mathbf{z}. \end{aligned}$$

We then remove the second-order information associated with the H_1 hypothesis from each individual channel by "whitening" with the filter $D_1^{-1/2}$ so that

$$\mathbf{z} \rightarrow \mathbf{w} = D_1^{-1/2} \mathbf{z}$$

$$E_{H_0}[\mathbf{w}\mathbf{w}^H] = D_1^{-1/2} D_0 D_1^{-H/2} = \Sigma^{-1}$$

$$E_{H_1}[\mathbf{w}\mathbf{w}^H] = D_1^{-1/2} R_{\mathbf{zz}_1} D_1^{-H/2} = E_1 = P_1 \Lambda_1 P_1^H$$

where the matrix Σ is in some sense a channel-wise signal-to-noise (SNR) matrix [15] with the jth diagonal block equal to

$$\Sigma_j = (R_{\mathbf{s}_{jj}} + R_{\mathbf{n}_j})^{H/2} R_{\mathbf{n}_j}^{-1} (R_{\mathbf{s}_{jj}} + R_{\mathbf{n}_j})^{1/2}.$$

The log-likelihood ratio in this new coordinate system then becomes

$$l(\mathbf{w}) = \mathbf{w}^H (\Sigma - P_1 \Lambda_1^{-1} P_1^H) \mathbf{w}.$$

Finally, we map the whitened data using the filter P_1 so that

$$\mathbf{w} \rightarrow \bar{\mathbf{v}} = P_1^H \mathbf{w}$$

$$E_{H_0}[\bar{\mathbf{v}}\bar{\mathbf{v}}^H] = P_1^H \Sigma^{-1} P_1$$

$$E_{H_1}[\bar{\mathbf{v}}\bar{\mathbf{v}}^H] = \Lambda_1$$

where Λ_1 is a matrix with the sum of the correlations among the mapped data (under H_1) along its diagonal. We can then rewrite the log-likelihood ratio as

$$l(\bar{\mathbf{v}}) = \bar{\mathbf{v}}^H (P_1^H \Sigma P_1 - \Lambda_1^{-1}) \bar{\mathbf{v}} \tag{13}$$

where $\bar{\mathbf{v}} = [\sum_{j=1}^N v_{1,j} \cdots \sum_{j=1}^N v_{d,j}]^T \in \mathbb{C}^d$ is a vector of the sum of the MCA coordinates under H_1. This is still the standard Gauss-Gauss log-likelihood ratio, but in the coordinates $P_1^H D_1^{-1/2} \mathbf{z}$ which allow us to measure the linear dependence among all N channels. MCA is used as a tool to "discover" the coherence structure among the channels by solving a generalized eigenvalue problem and the amount of coherence in each coordinate can then be determined through the eigenvalue λ_i.

Using (13) it is easy to show that the J-divergence measure of detectability [15] can be written as

$$\begin{aligned} J &= E_{H_1}[l(\bar{\mathbf{v}})] - E_{H_0}[l(\bar{\mathbf{v}})] \\ &= \mathrm{tr}(-2I + \Lambda_1 P_1^H \Sigma P_1 + \Lambda_1^{-1} P_1^H \Sigma^{-1} P_1) \\ &= \sum_{i=1}^{d} (-2 + \mathbf{p}_i^H [\lambda_i \Sigma + \lambda_i^{-1} \Sigma^{-1}] \mathbf{p}_i). \end{aligned} \tag{14}$$

As can be observed, the divergence in the MCA coordinate system becomes decomposed in terms of the MCA eigenvalue λ_i and two quadratic terms $\mathbf{p}_i^H \Sigma \mathbf{p}_i$ and $\mathbf{p}_i^H \Sigma^{-1} \mathbf{p}_i$. The quadratic term $\mathbf{p}_i^H \Sigma \mathbf{p}_i$ in some sense gives us a scalar measurement of the sum of the channel-wise SNRs in the 1-D subspace spanned by $\mathbf{p}_i$. Thus, writing the J-divergence in this manner decomposes the information needed for detection into the inter-relationships between data channels (λ_i) and the intra-relationships among the individual channels themselves ($\mathbf{p}_i^H \Sigma \mathbf{p}_i$).

REMARK 4 Throughout the rest of the paper we choose to disregard the intra-relationships of the channels and focus our attention around detecting the presence of coherence between the data channels by setting $\Sigma = I$. This results in the log-likelihood function

$$l(\bar{\mathbf{v}}) = \bar{\mathbf{v}}^H (I - \Lambda^{-1}) \bar{\mathbf{v}} \tag{15}$$

and J-divergence

$$J = \sum_{i=1}^{d} (-2 + \lambda_i + \lambda_i^{-1}) \tag{16}$$

which are similar to those given in [15]. Additionally, doing so substantially simplifies the implementation of the detector as it becomes independent of prior characterization of matrix Σ. This simplification is particularly useful for the implementation of the reduced-rank detector described next.

Note that in situations where d is large, it can be advantageous to implement a reduced-rank version of the likelihood ratio given in (15) by finding the best rank-r approximation $\tilde{E}$ of the coherence matrix E. This not only reduces the computational requirement from $\mathcal{O}(d^2)$ operations to $\mathcal{O}(r^2)$ when computing the likelihood function but also improves detection performance by eliminating coordinates that do not contribute any discriminatory information for detection. For the remainder of this section, all hypothesis-specific subscripts are dropped with the understanding that it theoretically applies to hypothesis H_1. Typically one builds this approximation from the eigenmodes of E associated with the largest r eigenvalues, i.e., $\tilde{E} = \sum_{i=1}^r \lambda_i \mathbf{p}_i \mathbf{p}_i^H$ where $\lambda_1 > \cdots > \lambda_r > \cdots > \lambda_d$. By the Eckart-Young Theorem [16], this choice for $\tilde{E}$ is optimal in the sense that it minimizes the mean-squared error $\|E - \tilde{E}\|_F^2$. However, rather than using mean-squared error as a performance criterion for rank reduction, we take the approach presented in [15] and choose $\tilde{E}$ to maximize J-divergence, a performance measure which is undoubtedly more aligned with detection. Without loss of generality, we now assume that the eigenvectors $\mathbf{p}_1, \ldots, \mathbf{p}_d$ of the coherence matrix E are sorted in a descending fashion such that $\lambda_1 + \lambda_1^{-1} > \cdots > \lambda_d + \lambda_d^{-1}$ and we form the matrices $P_r = [\mathbf{p}_1 \cdots \mathbf{p}_r]$ and $\Lambda_r = \mathrm{diag}[\lambda_1, \ldots, \lambda_r]$. There are many possible methods for choosing a suitable value for r. Here we choose r according to the following criterion

$$r = \arg\min\{p : J_p / J \geq 1 - \epsilon\} \tag{17}$$

where ϵ is a preselected small quantity and J_p denotes the J-divergence after discarding coordinates $p+1, \ldots, d$

$$J_p = \sum_{i=1}^{p} (-2 + \lambda_i + \lambda_i^{-1}). \tag{18}$$

In other words, we choose the smallest set of coordinates that maintains a significant percentage of the original J-divergence. Eigenvectors associated with eigenvalues which are either large or extremely small in value typically get chosen to be included in P_r, a fact we empirically motivate in Section IV. Having chosen a suitable value for r, we then form the vector $\bar{\mathbf{v}}_r = P_r^H \mathbf{w} = [\sum_{j=1}^N v_{1,j} \cdots \sum_{j=1}^N v_{r,j}]^T \in \mathbb{C}^r$ and apply it to the reduced-rank version of the log-likelihood function

$$l(\bar{\mathbf{v}}_r) = \bar{\mathbf{v}}_r^H (I_r - \Lambda_r^{-1}) \bar{\mathbf{v}}_r. \tag{19}$$

IV. TEST RESULTS

A. Data Description

The MCA-based coherence detector is applied to a four-channel sonar data set consisting of one HF high-resolution side-scan image as well as three BB sonar images which all cover the same region on the seafloor with the images captured from multiple target fields. Coregistration of these sonar systems is guaranteed as both HF and BB sonar are mounted on the same autonomous underwater vehicle (AUV)

and use the same receiver array. The pinging for the HF and BB sonar systems is done simultaneously as they are sufficiently far apart in frequency such that the returns are easily separable. The three BB sonar images used for this study are formed by bandpass filtering the returns from the BB sonar to extract three nonoverlapping frequency subbands, each associated with one BB sonar image. Thus, the sonar images used in this study are disparate in frequency content and resolution but not in location, elevation, or aspect. Each image is complex-valued and generated at the output of the k-space or wavenumber beamformer [9]. The image database contains 59 coregistered sonar images with each image consisting of both port and starboard-side images. The database contains 53 targets with some images containing more than one target. Because the HF sonar provides higher spatial resolution and better ability to capture target details and characteristics while the BB sonar offers much better clutter suppression ability with lower spatial resolution, detectors were run using HF images along with one or more of the BB sonar images to ensure a high probability of detection with a low false alarm rate. Three different cases were implemented, a two-channel detector with the HF sonar image along with one of three BB sonar images (referred to as HF-BB_1), a three-channel detector with the HF sonar image, the same BB sonar, and a different BB sonar image (referred to as HF-BB_1-BB_2), and finally a four-channel with the HF sonar image and all three BB sonar images (referred to as HF-BB_1-BB_2-BB_3). The goal of this study is to determine the impact different combinations and numbers of HF and BB sonar systems have on the detection performance and establish the point of diminishing returns.

B. Data Preparation and Preprocessing

When processing the images in the data sets for the MCA-based detector, each set of N ($N = 2$, 3, or 4 for this study) images is first partitioned into coregistered ROIs with 50% overlap in both the vertical and horizontal directions. ROIs are formed in an overlapping fashion to ensure that the target will not be split among different ROIs. Thus, if an ROI contains a target, it will encompass the entirety of the target structure. Based on the average target size, ROIs pertaining to HF images are chosen to be 72 pixels tall by 112 pixels wide. Because of differences in beamwidth in HF and BB sonar leading to discrepancies in image resolution, the ROIs pertaining to BB images are not the same size and are chosen to be 24 pixels tall by 224 pixels wide. This choice of ROI sizes ensures proper correspondence among the HF and BB images. Once the set of N coregistered ROIs has been extracted

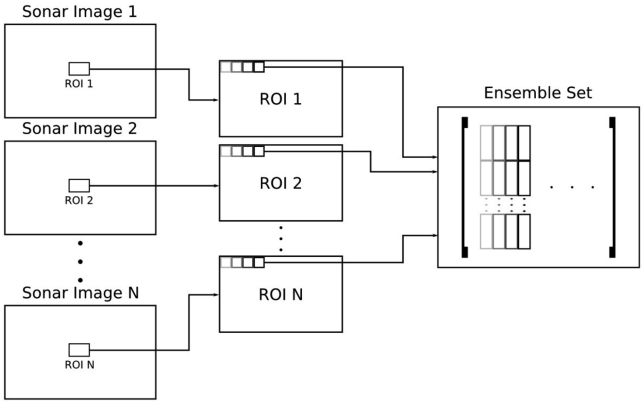

Fig. 2. Sonar data preprocessing.

from each of the N sonar images, each ROI is partitioned into nonoverlapping blocks of size 6×4 for HF images and 2×8 for BB. The difference in block size for each sonar type is a byproduct of their differences in resolution. Corresponding blocks in the ROIs are then reshaped into vectors and concatenated to form the composite observation vector $\mathbf{z}$ defined in Section II. An ensemble set is then formed from all 336 blocks ($72 \times 112/6 \times 4 = 24 \times 224/2 \times 8 = 336$) in each set of N coregistered ROIs. Figure 2 gives a graphical overview of the ROI formation, blocking, and ensemble preprocessing steps used to prepare the multi-channel sonar data for detection.

One of the obvious practical limitations of the detection method described in this paper is the issues that arise when the data from all N channels is not sufficiently coregistered. A severe lack in coregistration will undoubtedly lead to poorer detection performance under most circumstances. However, this issue does motivate the use of blocks within the ROI leading to observations that lie in a higher dimensional space as it makes the detector more robust to small deviations in coregistration. This added robustness is no doubt due to the fact that, in this situation, we are characterizing the statistical relationships among all the pixels within that block rather than only considering the scalar covariance information of the pixels themselves. So heuristically speaking, as long as the deviation in coregistration is relatively small, then a sufficiently large block size should still do a good job at capturing the mutual information among the channels. However, if the lack in coregistration is sizable then one would have to consider a preprocessing step that accounted for propagation delays and possibly even Doppler shifts (e.g. radar applications). This could be accomplished by fixing one channel as a reference and correlating it with the others over a range of different temporal/spatial lags and Doppler shifts, i.e., a matched filter, for situations without prior knowledge of this mismatch.

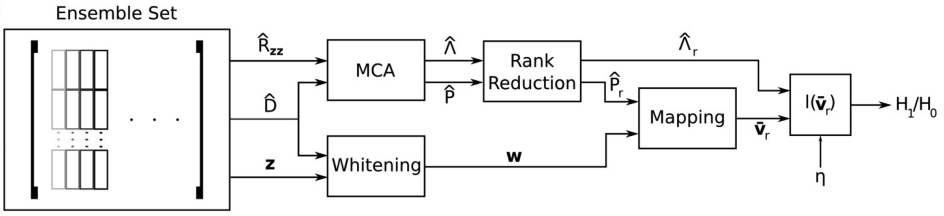

Fig. 3. MCA detection system.

C. MCA Detection

Once the ensemble set is built from the blocks from all N ROIs, it is then used to form an estimate of the composite covariance matrix $\hat{R}_{\mathbf{zz}}$ (here "$\hat{}$" is used to denote the sampled version of this matrix) along with its block diagonal counterpart $\hat{D}$. These matrices are then used to find the estimated sum of correlations and MCA mapping matrices, $\hat{\Lambda}$ and $\hat{P}$, respectively, using the eigenvalue problem given in (5). Both $\hat{\Lambda}$ and $\hat{P}$ are then applied to the rank-reduction procedure described at the end of Section III to form the matrices $\hat{\Lambda}_r$ and $\hat{P}_r$ needed to form the log-likelihood ratio test statistic given in (19) for that particular set of N ROIs. To form the log-likelihood ratio, each observation vector $\mathbf{z}$ from the ensemble set is whitened and mapped, using the filters $\hat{D}$ and $\hat{P}_r$, respectively, to generate the vector $\tilde{\mathbf{v}}_r = \hat{P}_r^H \mathbf{w} = \hat{P}_r^H \hat{D}^{-1/2} \mathbf{z}$ used in (19). The values of the log-likelihood ratio for each block are then averaged over all 336 realizations and compared with a threshold η to form a decision for that ROI. Figure 3 gives a graphical overview of the MCA detection process just described.

To show the statistics of the multi-channel correlations for ROIs that contain targets immersed in background and those that solely contain background, a test was conducted on the entire set of 53 targets corresponding to 212 ROIs (note that as a result of the 50% overlap in ROI formation, there are essentially 4 ROIs that contain the same target leading to a total of $53 \times 4 = 212$ ROIs) and a same size randomly selected set of 212 ROIs containing only background clutter. Figures 4(a)–(c) exhibit plots of the mean and standard deviation of all d multi-channel correlations λ_i, $i = 1,\ldots,d$, of ROIs containing targets and those containing only background for the HF-BB_1 ($d = 40$), HF-BB_1-BB_2 ($d = 56$), and HF-BB_1-BB_2-BB_3 ($d = 72$) detectors, respectively. Mean values for each λ_i are shown by the solid line whereas the length of the bar denotes its corresponding standard deviation. Note that the symmetry of the correlation values observed in Fig. 4(a) and the fact that $\lambda_{17} = \cdots = \lambda_{24} = 1$ are a result of the arguments made in Remark 3. As can be seen, there is suitable separation among both the largest and smallest correlation values corresponding to targets versus those corresponding to background clutter alone as there is a noticeable difference in mean values. However, as the value of λ_i approaches unity the separation among target and background begins to diminish. Recalling the arguments given at the end of Section III, we can now see that performing rank reduction by minimizing mean-squared error inherently ignores those coordinates associated with small eigenvalues which do, in fact, contain a suitable amount of discriminatory information for detection. On the other hand, maximizing J-divergence involves retaining coordinates associated with eigenvalues which are both large and small thus giving one a much better performance criteria for implementing low-rank detection.

D. GLRT Detector as a Benchmark

For the purposes of comparison, the GLRT detector in [3] is also implemented on the same 2, 3, and 4 channel sonar data sets. The preprocessing for this detector uses the same steps as described in Section IV-B, namely ROI formation, ROI blocking, and the formation of an ensemble to estimate $R_{\mathbf{zz}}$. Taking the same composite covariance matrix $\hat{R}_{\mathbf{zz}}$ estimated from the ensemble set built from all 336 blocks in the set of ROIs, the test statistic for the GLRT can be written as the following generalized Hadamard ratio

$$l(\hat{R}_{\mathbf{zz}}) = \frac{\det(\hat{R}_{\mathbf{zz}})}{\prod_{j=1}^{N} \det(\hat{R}_{jj})}$$

with $\hat{R}_{jj}$ representing the diagonal blocks of $\hat{R}_{\mathbf{zz}}$ and "$\hat{}$" denoting the sampled version of the associated matrix. This likelihood ratio can then be rewritten [3] as

$$l(\hat{R}_{\mathbf{zz}}) = \det(\hat{D}^{-1/2} \hat{R}_{\mathbf{zz}} \hat{D}^{-H/2}) = \det(\hat{E})$$

where $\hat{E}$ is the estimated coherence matrix defined in (5). As a result, the GLRT shares the following relationship with the MCA correlations

$$l(\hat{R}_{\mathbf{zz}}) = \prod_{i=1}^{d} \hat{\lambda}_i$$

where $\hat{\Lambda} = \mathrm{diag}(\hat{\lambda}_1,\ldots,\hat{\lambda}_d)$. When implementing the detector, the likelihood ratio is applied to the monotonically decreasing transformation $-\ln(x)$

$$-\ln[l(\hat{R}_{\mathbf{zz}})] = -\sum_{i=1}^{d} \ln(\hat{\lambda}_i) \tag{20}$$

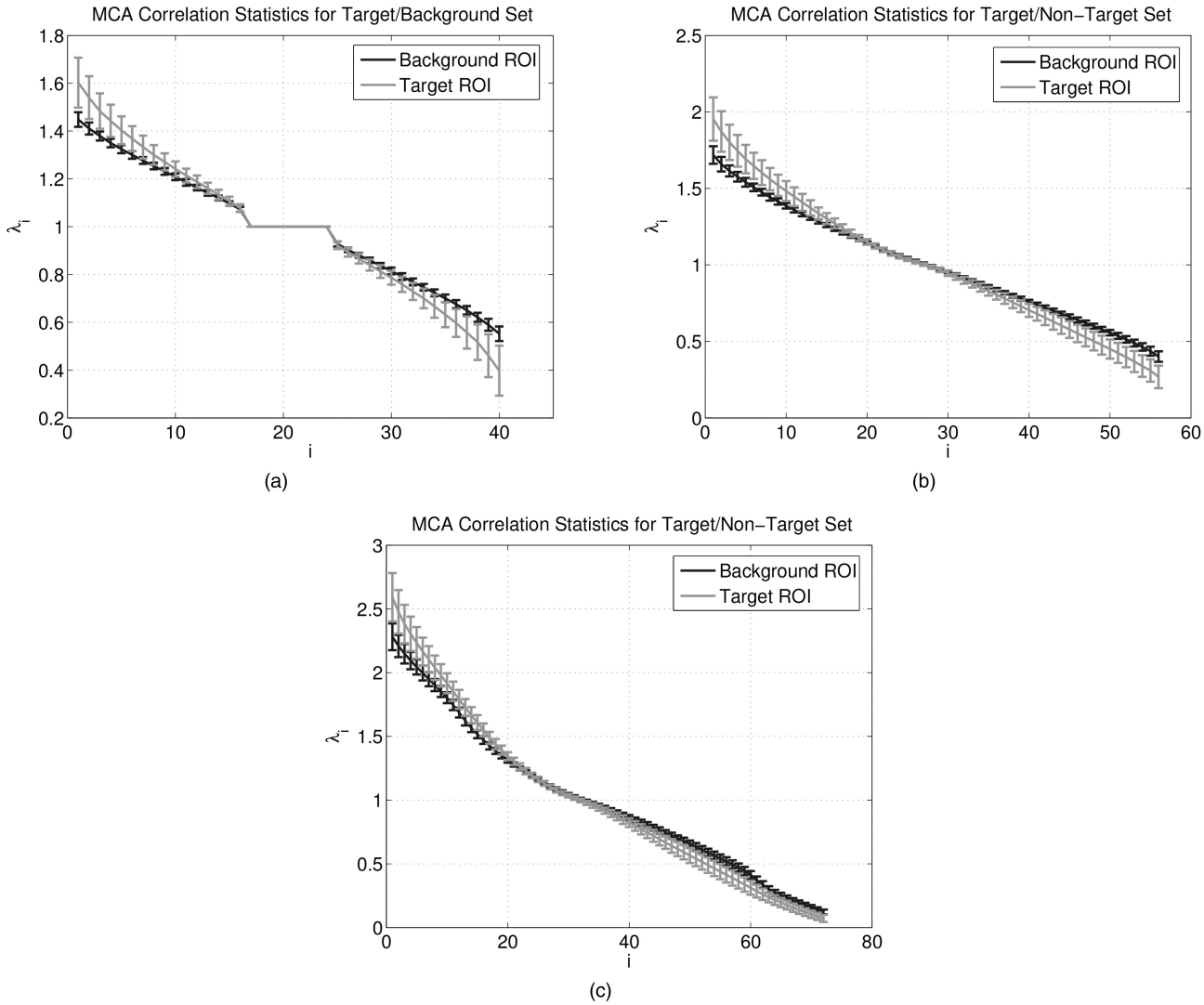

Fig. 4. Statistics of MCA correlations for all channel configurations. (a) HF-BB_1 detector. (b) HF-BB_1-BB_2 detector. (c) HF-BB_1-BB_2-BB_3 detector.

which is shown in [11] to represent the mutual information among N multivariate Gaussian channels. Thus, the larger the estimated mutual information, the more coherence among all N channels and the more likely the presence of a target.

It was noted in both [2] and [3] that the above likelihood ratio can be related to a simpler ad hoc detector based on the norm of the estimated coherence matrix when the channels exhibit low coherence or equivalently low SNR. In such a situation the eigenvalues of the estimated coherence matrix can be modeled as small perturbations from unity, i.e., $\hat{\lambda}_i = 1 + \epsilon_i$ where $|\epsilon_i| \ll 1$. Using the Taylor series expansion of $\ln(1+x)$ up to second-order and noting that the squared Frobenius norm of a Hermitian matrix is the sum-squared of its eigenvalues, the log-likelihood ratio can be written

$$-\ln[l(\hat{R}_{\mathbf{zz}})] \approx \frac{1}{2}\|\hat{E}\|_F^2 - \frac{d}{2}. \tag{21}$$

In [2] and [3] it was noted that this alternative log-likelihood measurement is simpler to compute (only $\mathcal{O}(d^2)$ operations to compute a Frobenius norm versus $\mathcal{O}(d^3)$ to compute a determinant) and as a consequence forms a more robust test statistic under these circumstances. In the results that are to follow, we not only compare the proposed detection method with the GLRT given in (20) but also it's low SNR approximation given in (21).

E. Rank Reduction Studies

To investigate the effects of rank reduction on the performance of the detector, a test was conducted to observe the detector's sensitivity to varying values of the parameter ϵ given in (17). To achieve this, for every $\epsilon \in [0, 0.5]$, a receiver operating characteristic (ROC) curve is formed using the reduced rank likelihood ratio given in (19) and the area under the ROC curve (AUC) computed with larger values of AUC signifying better detection performance. Figure 5

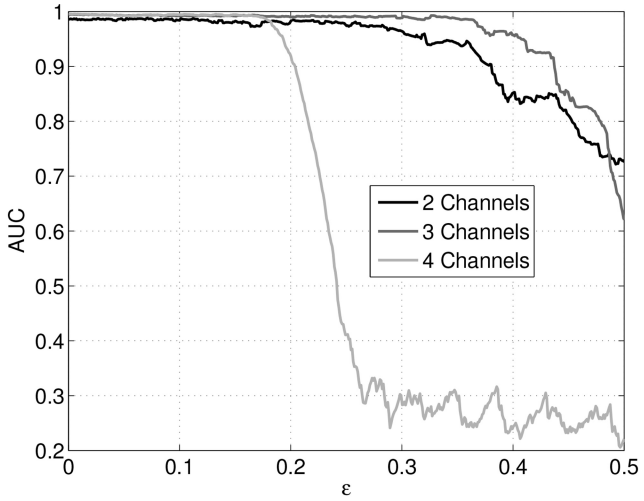

Fig. 5. AUC versus ϵ.

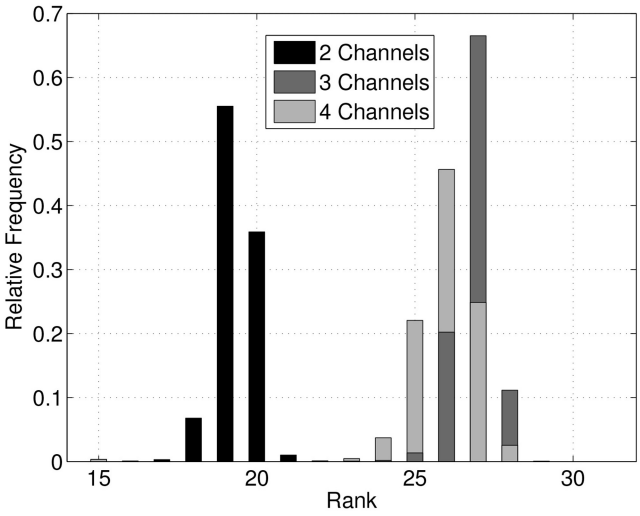

Fig. 6. Rank histograms for $\epsilon = 0.1$.

displays AUC versus ϵ for all three MCA-based detectors. From the figure we can see that both the two- and three-channel detectors remain robust to rank reduction as both achieve 0.9 AUC while maintaining only approximately 65% of their full rank J-divergence. However, adding the third broadband channel to the three-channel detector results in a detector much more sensitive to the effects of rank reduction.

Looking again at Fig. 5, we notice that none of the detectors exhibit significant deterioration in performance for $\epsilon \leq 0.1$. For this reason $\epsilon = 0.1$ was chosen as a suitable operating point for the rank reduction procedure, i.e., the rank of the detectors is chosen to achieve 90% of its full rank J-divergence. Figure 6 displays histograms of the rank for all ROIs in the dataset. From this figure it is evident that adding the third broadband channel to the three-channel detector brings little information to the detector as, even though we have augmented our observation with an additional 16-dimensional vector, we see little change in the rank of the detector when going from three to four channels. From this study we can see that the proposed method is effective at reducing the rank of these detectors with a reduction by a factor of 2 for the two- and three-channel detectors and a factor of 3 for the four-channel detector.

F. Detection Results

Using all ROIs in the dataset, ROC curves for the MCA detector given in (19), the GLRT detector given in (20) (denoted "GLRT-LogDet"), and its low-SNR approximation given in (21) (denoted "GLRT-FrobNorm") are generated and presented in Figs. 7(a)–(c) for all three channel configurations. As can be seen, at the knee point of the ROC (where $P_d + P_{fa} = 1$ denoted by circles in Figs. 7(a)–(c)) the MCA-based three-channel detector provided an increase in performance over that of the two-channel detector as the two-channel detector exhibits $P_d = 94\%$ at the knee point of the ROC curve whereas that of the three-channel detector gives $P_d = 96\%$. Likewise, both the GLRT as well as its approximation exhibit an increase in knee point probability going from $P_d = 91\%$ for both two-channel detectors to $P_d = 96\%$ for their three-channel versions. However, when adding the last broadband channel to these three channel detectors, we see no increase in knee point probability as the MCA as well as both GLRT detectors maintain $P_d = 96\%$. Additionally, with the exception of the two-channel case where the MCA-based detector provided a 3% improvement in knee point P_D over the two GLRT detectors, we can see that all three methods exhibit fairly similar ROC performance.

To select a suitable threshold for detection, 12 images (approximately 10% of the dataset) devoid of any target were chosen at random from the dataset and used to determine the threshold needed to falsely detect only 2% of the ROIs within an image on average, a realistic operating point for this application. With the 12 randomly chosen images included, the MCA as well as both GLRT detectors were then tested on the entire dataset using these thresholds. Table I displays the thresholds, the number of targets correctly detected, and the average percentage of ROIs falsely detected within an image for all three detection methods and for all three channel configurations. From this table we can see that the MCA two-channel detector as well as both GLRT two-channel detectors exhibit similar performance at this operating point as all three detect 44 targets ($P_d = 83\%$). When adding an additional broadband channel to these detectors we see significant improvement as the MCA method detects 48 targets ($P_d = 91\%$) and the GLRT and its approximation detect 46 targets ($P_d = 87\%$). Finally, when adding the last broadband

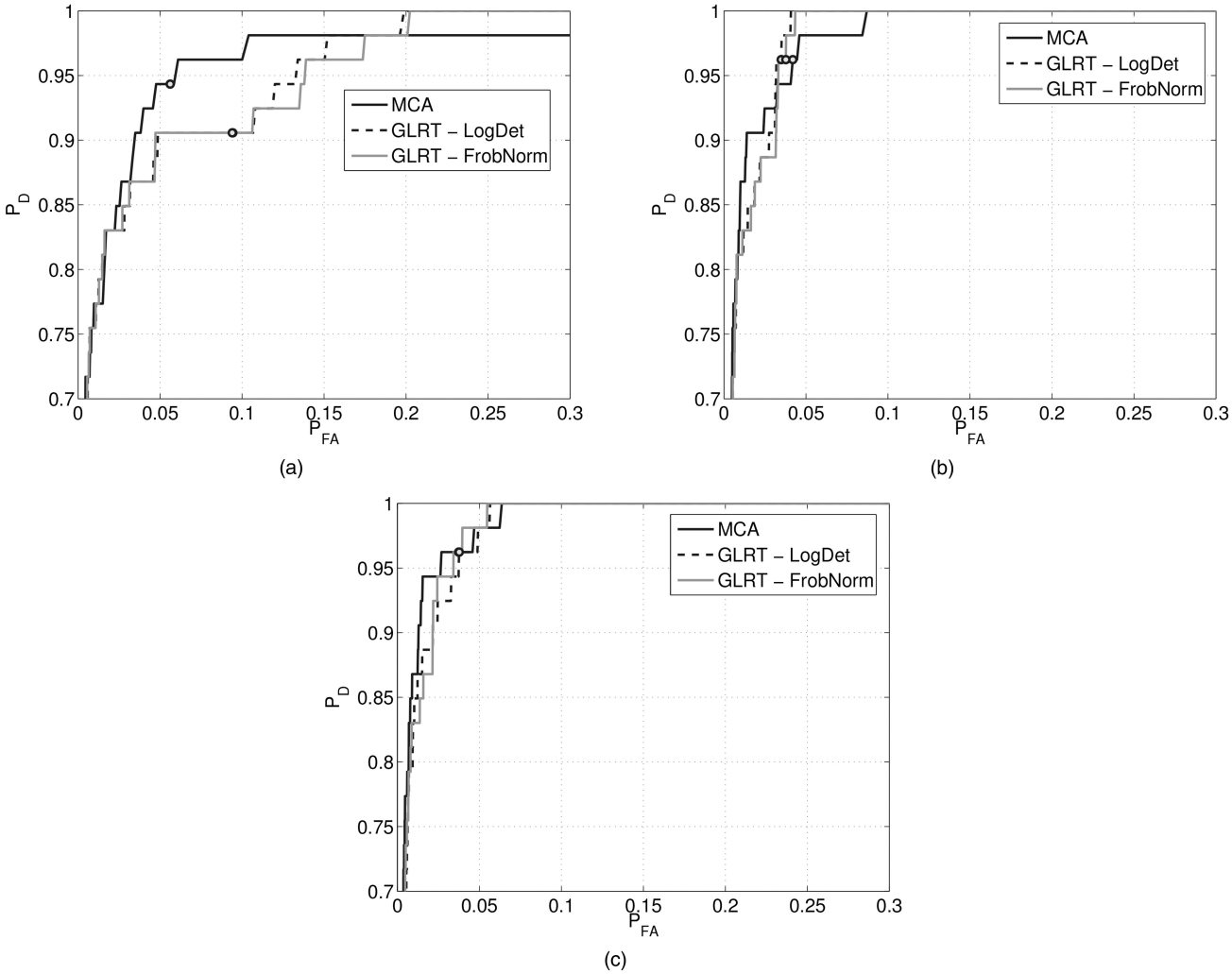

Fig. 7. ROC curves for all channel configurations. (a) Two-channel ROC curves. (b) Three-channel ROC curves. (c) Four-channel ROC curves.

TABLE I
Multi-Platform Detection Results

Channels	Detector	Threshold	Targets Detected	% False Alarms per Image
HF-BB_1	MCA	−1.13	44	1.77
	GLRT-LogDet	1.66	44	1.94
	GLRT-FrobNorm	1.52	44	1.95
HF-BB_1-BB_2	MCA	−2.58	48	1.91
	GLRT-LogDet	4.73	46	2.11
	GLRT-FrobNorm	4.26	46	2.10
HF-BB_1-BB_2-BB_3	MCA	−6.14	50	1.93
	GLRT-LogDet	18.20	47	1.87
	GLRT-FrobNorm	13.72	46	1.88

channel to the three channel detectors we only observe marginal improvement as the MCA method detects an additional two targets (P_d = 94%), the GLRT detects an additional target (P_d = 89%), and the GLRT approximation maintains the same detection rate as its three-channel counterpart. From the table we can also see that the false alarm rates for all three methods do in fact remain robust to the inclusion of additional data as they all come close to the average false alarm percentage that was desired.

V. CONCLUSION

This paper develops a new detection method exploiting the coherence among multiple sensing systems that could be disparate in location, frequency, resolution, etc. The MCA framework provides the ideal coordinate system for implementing such a detection system by finding sets of basis vectors which maximize the sum of the correlations among all pair-wise combinations of channels, thus "discovering" the amount of coherence among multiple observations. The detector for Gaussian random vectors is then cast into the MCA framework by writing the log-likelihood ratio and J-divergence in terms of the MCA variates. A rank-reduced version of this detector is then derived by enforcing simplifying assumptions on the structure of a channel-wise SNR

matrix and then finding the low-rank approximation of the MCA coherence matrix that captures a certain percentage of the full-rank J-divergence measure. This reduced-rank MCA-based detector is then applied to a multi-sonar data set consisting of one HF sonar image and three BB sonar images coregistered over the same region on the seafloor and compared with a GLRT detector and its low-SNR approximation. Taking advantage of the inherent characteristics of HF and BB sonar, three cases were tested for the three detection methods with one HF image and one to three BB images to study the detector's response to a varying number of channels. It was observed that there was little if any improvement in ROC characteristics when moving from the three-channel detector to the four-channel detector. Moreover, it was observed that the inclusion of this additional BB channel brought no increase in the rank over that of the three-channel detector. This lack of improvement in performance may be attributed to the fact that all BB images were bandpass filter versions of the same signal and therefore contain essentially similar information. It must be noted, however, that the data set used in this paper contained an extremely limited number of realizations of the H_1 hypothesis with a total of only 53 targets. However, from the limited realizations of targets in this data set we can see that the proposed method builds low rank detectors that are capable of achieving $P_D = 94\%$ with the inclusion of all HF and BB images while falsely detecting only 2% of the ROIs within an image on average.

ACKNOWLEDGMENT

The authors would like to thank NSWC–Panama City Division for support and providing the data used in this study.

REFERENCES

[1] Cochran, D., Gish, H., and Sinno, D.
A geometric approach to multiple-channel signal detection.
IEEE Transactions on Signal Processing, **43** (Sept. 1995), 2049–2057.

[2] Leshem, A. and Van der Veen, A. J.
Multichannel detection of Gaussian signals with uncalibrated receivers.
IEEE Signal Processing Letters, **8**, 4 (2001), 120–122.

[3] Ramirez, D., et al.
Detection of spatially correlated Gaussian time series.
IEEE Transactions on Signal Processing, **58**, 10 (2010), 5006–5015.

[4] Hotelling, H.
Relations between two sets of variates.
Biometrika, **28** (1936), 321–377.

[5] Scharf, L. and Mullis, C.
Canonical coordinates and the geometry of inference, rate, and capacity.
IEEE Transactions on Signal Processing, **48**, 3 (Mar. 2000), 824–891.

[6] Pezeshki, A., et al.
Canonical coordinates are the right coordinates for low-rank Gauss-Gauss detection and estimation.
IEEE Transactions on Signal Processing, **54**, 12 (Dec. 2006), 4817–4820.

[7] Cartmill, J., Wachowski, N., and Azimi-Sadjadi, M. R.
Buried underwater object classification using a collaborative multi-aspect classifier.
IEEE Journal of Oceanic Engineering, **34**, 1 (2009), 32–44.

[8] Wachowski, N. and Azimi-Sadjadi, M. R.
Buried underwater target classification using frequency subband coherence analysis.
Proceedings of the MTS/IEEE Oceans 2008 Conference, Oct. 2008, pp. 1–8.

[9] Tucker, J. D. and Azimi-Sadjadi, M. R.
Coherence-based underwater target detection from multiple disparate sonar platforms.
IEEE Journal of Oceanic Engineering, **36**, 1 (Jan. 2011), 38–52.

[10] Kettenring, J. R.
Canonical analysis of several sets of variables.
Biometrika, **58** (1971), 433–451.

[11] Thompson, B. D. and Azimi-Sadjadi, M. R.
Iterative multi-channel coherence analysis with applications.
Neural Networks, **21**, 2–3 (2008), 493–501.

[12] Neilsen, A.
Multiset canonical correlations analysis and multispectral, truly multitemporal remote sensing data.
IEEE Transactions on Image Processing, **11** (Mar. 2002), 293–305.

[13] Via, J., Santamaria, I., and Perez, J.
A learning algorithm for adaptive canonical correlation analysis of several data sets.
Neural Networks, **20**, 1 (Jan. 2007), 139–152.

[14] Golub, G. H. and Van Loan, C. F.
Matrix Computations (3rd ed.).
Baltimore, MD: Johns Hopkins University Press, 1996.

[15] Scharf, L. L. and Van Veen, B. D.
Low rank detectors for Gaussian random vectors.
IEEE Transactions on Acoustics, Speech, and Signal Processing, **35**, 11 (Nov. 1987), 1579–1582.

[16] Johnson, R.
On a theorem stated by Eckart and Young.
Psychometrika, **28**, 3 (Sept. 1963), 259–263.

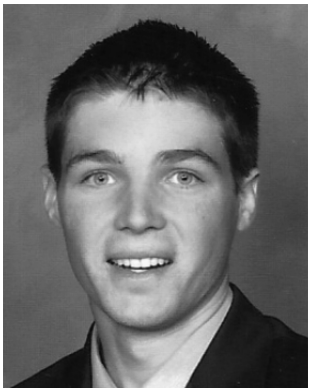

Nick Klausner (S'08) received B.S. degrees in electrical engineering and economics from the Colorado School of Mines, Golden, CO in 2008 and the M.S. degree in electrical and computer engineering from Colorado State University, Fort Collins, CO in 2010.

Since 2010 he has been working towards the Ph.D. degree in electrical and computer engineering at Colorado State University under the direction of Dr. Azimi-Sadjadi. His current research interests include statistical signal processing, digital signal processing, and digital image processing.

Mahmood R. Azimi-Sadjadi (M'81—SM'89) received the M.S. and Ph.D. degrees from the Imperial College of Science and Technology, University of London, London, U.K., in 1978 and 1982, respectively, both in electrical engineering with specialization in digital signal/image processing.

He is currently a full professor with the Electrical and Computer Engineering Department, Colorado State University (CSU), Fort Collins. He is also serving as the Director of the Digital Signal/Image Laboratory at CSU. His main areas of interest include statistical signal and image processing, target detection, classification and tracking, sensor array processing, learning systems, and distributed sensor networks.

Dr. Azimi-Sadjadi is the coauthor of the book, *Digital Filtering in One and Two Dimensions* (Plenum Press, 1989). He served as an Associate Editor of the *IEEE Transactions on Signal Processing* and the *IEEE Transactions on Neural Networks*.